Guided waves in marine CSEM and the adjustment distance in MT: a synopsis

Peter Weidelt
Institut für Geophysik und Extraterrestrische Physik
Technische Universität Braunschweig
D-38106 Braunschweig, Germany
E-mail: p.weidelt@tu-bs.de

1. Introduction

The Controlled Source Electromagnetic Method (CSEM) has recently found some interest in off-shore hydrocarbon exploration: An electric dipole with a transient or low-frequency continuous wave excitation is towed over an array of seafloor receivers measuring the electric and/or magnetic field. The target is a deep resistive layer as possible indicator for the presence of a hydrocarbon reservoir. The present study is confined to continuous wave excitation (with a typical frequency of 0.5 Hz) and to electric field data. A more detailed presentation of the CSEM results is given by Weidelt (2007).

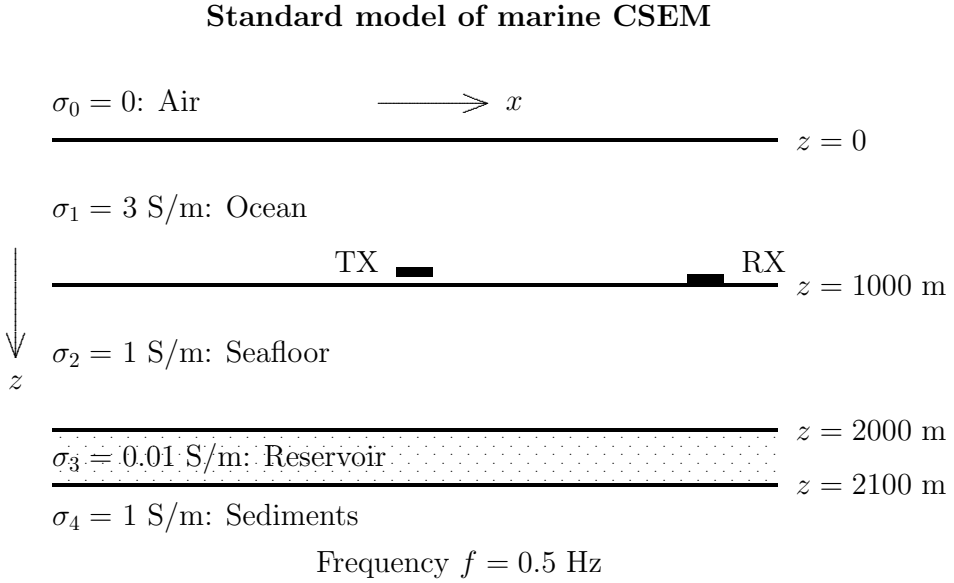

Ways of energy propagation between TX **and** RX**:**
- direct
- along air-earth interface ('airwave')
- resistive layer mode

Figure 1: Experimental setup and standard conductivity model for CSEM. The receiver TX measures the electric field. Used is both the inline configuration (as shown) and the broadside configuration with RX parallel to TX, but off the plane on the y-axis.

It turns out that the model shown in Fig. 1 has much in common with the resistive-layer distortion of the electric field in magnetotellurics (MT) due to the presence of a conducting

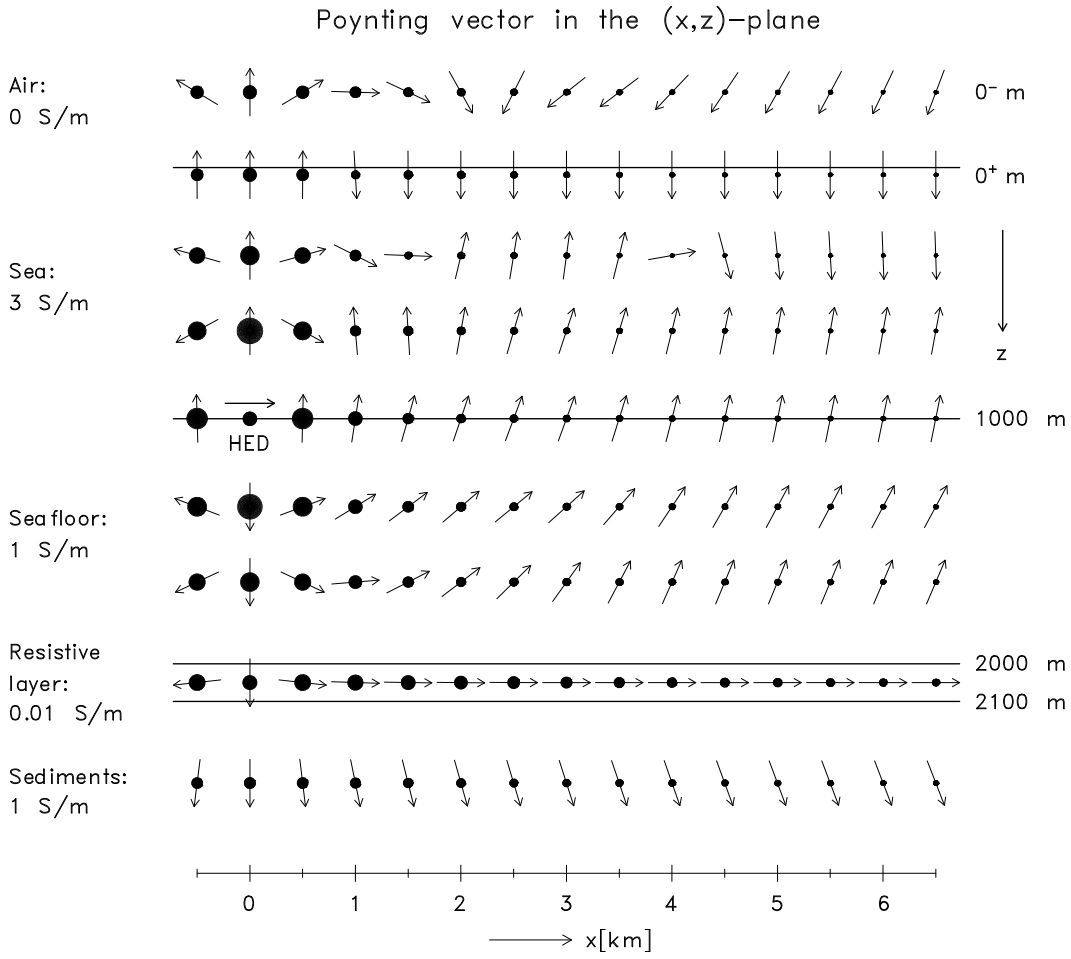

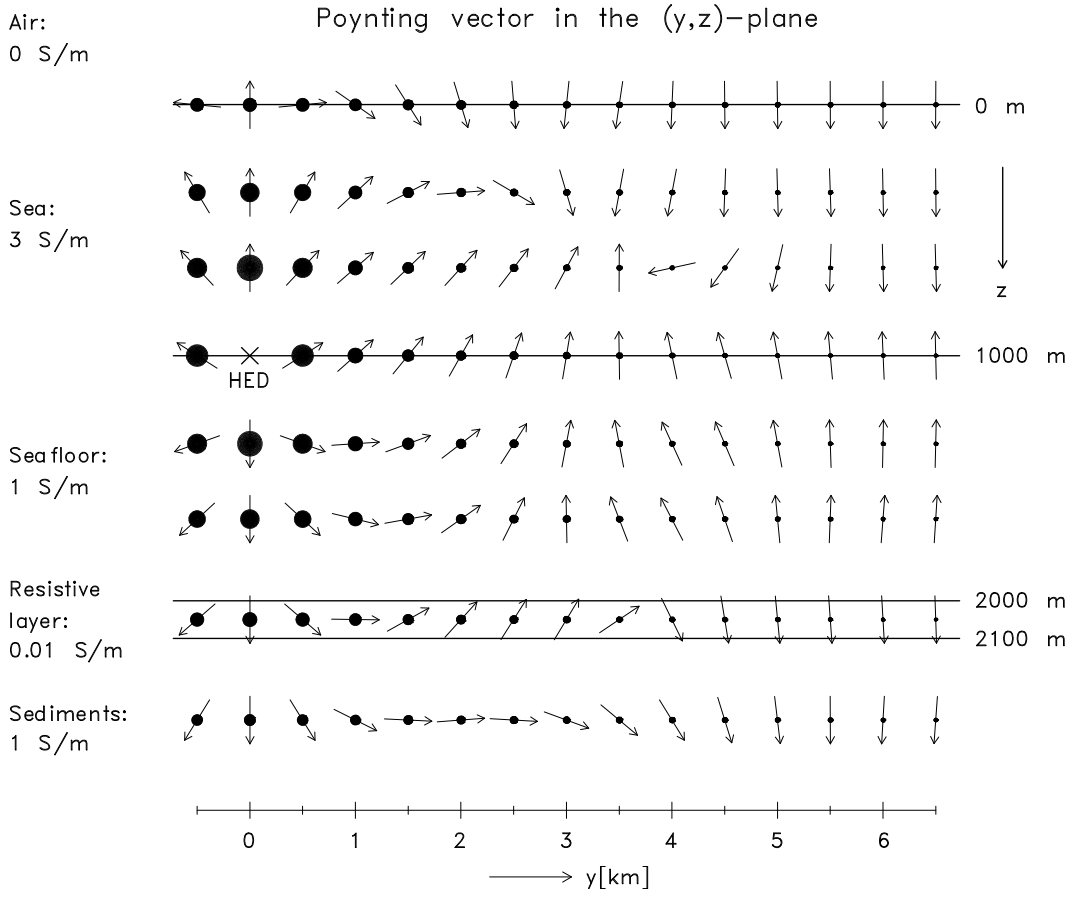

Figure 2: Energy flow density (Poynting vector) in two orthogonal planes

laterally nonuniform conductivity anomaly. Here the electric field can attain its asymptotic layered-earth values only at a very great distance from the anomaly. This distance is the so-called *adjustment distance*. It will be briefly discussed in Sect. 5.

For the representative model of Fig. 1, the time-averaged energy flow density (= Poynting vector) is shown in Fig. 2, both in the plane containing the horizontal electric dipole (top) and in the plane orthogonal to it (bottom) in Fig. 2.

The time averaged real Poynting vector

$$\overline{\mathbf{S}} := \frac{1}{2}\mathrm{Re}(\mathbf{E} \times \mathbf{H}^*)$$

reads in the (x, z)-plane at $y = 0$ (top of Fig. 2):

$$\overline{S}_x = -\frac{1}{2}\mathrm{Re}(E_z H_y^*), \quad \overline{S}_z = +\frac{1}{2}\mathrm{Re}(E_x H_y^*)$$

and in the (y, z)-plane at $x = 0$ (bottom of Fig. 2):

$$\overline{S}_y = -\frac{1}{2}\mathrm{Re}(E_x H_z^*), \quad \overline{S}_z = +\frac{1}{2}\mathrm{Re}(E_x H_y^*).$$

Of relevance for the physics of CSEM and the interpretation of seafloor data are two guided waves, namely the airwave and the resistive-layer mode:

- **Airwave**
  The airwave is guided at the air-ocean interface with a decay $\sim 1/r^3$ for great TX-RX separations r. In Fig. 2 the airwave is dominant, where close to the interface the flow of energy is vertical. For shallow water depth the strong airwave masks the signal from the target layer. The airwave is a TE-mode. In marine CSEM it has to be considered as noise.

- **Resistive-layer mode**
  This exponentially decaying mode (typical decay length 1700 m) is seen only in the plane containing the dipole (Fig. 2, top). It is associated with a strong horizontal energy flow, carried in the resistive layer by H_y and the strong component E_z. It is a TM-mode and contains the useful signal.

2. The airwave

In the sequel cylindrical coordinates (r, φ, z) are used. Attention is confined to the 'inline configuration', i.e. to the measurement of the radial component E_r in direction of the electric dipole. Moreover, the field is normalized with the current moment p of the dipole. Fig. 3 displays the modulus of $E_r(r)/p$ as a function of the TX-RX separation r for various depths d_1 of the sea water. In this log-log plot the airwave with its $1/r^3$-decay is easily visible as a straight line section in the farfield. The resistive-layer mode is clearly visible only at the great water depth d_1 =1000 m as the concave feature in the range 1 km< r <10 km; for shallower depth it is partly masked by the airwave.

For a 1D conductivity distribution $\sigma(z) > 0$ in $z > 0$ with source at depth z_0, receiver at depth z, angular frequency $\omega = 2\pi f$ and current moment p, the leading term of the airwave is given by

$$E_r^{air}(\mathbf{r}) = \frac{i\omega\mu_0\, p\cos\varphi}{2\pi r^3} \cdot \frac{e(z)\, e(z_0)}{[\, e'(0)\,]^2}, \quad E_\varphi^{air}(\mathbf{r}) = \frac{i\omega\mu_0\, p\sin\varphi}{\pi r^3} \cdot \frac{e(z)\, e(z_0)}{[\, e'(0)\,]^2} \tag{1}$$

where $e(z)$ is the downward diffusing solution of

$$e''(z) = i\omega\mu_0\sigma(z)\, e(z). \tag{2}$$

Physically, $e(z)$ is the electric field in 1D magnetotellurics.

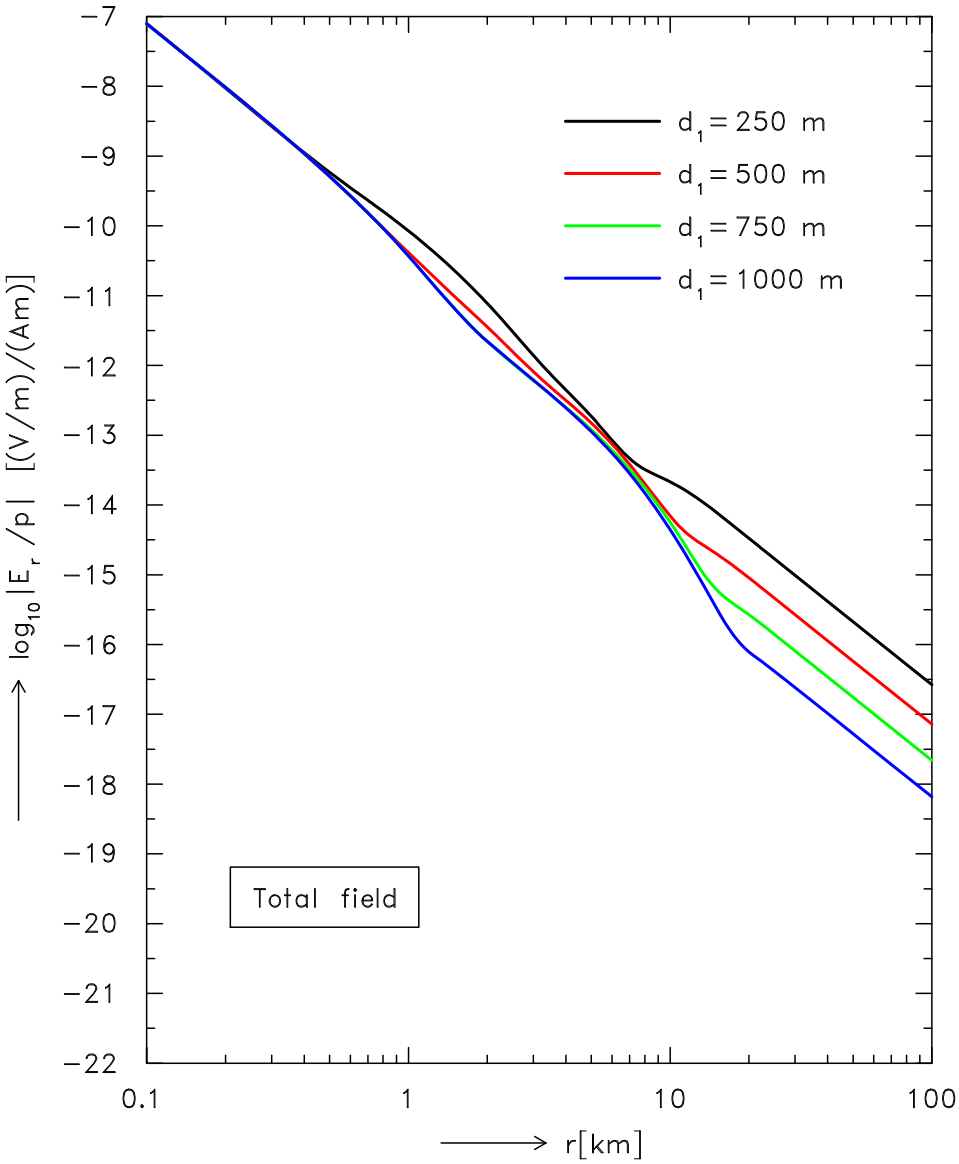

Figure 3: Radial component E_r of the electric field, normalized with the current moment p of the electric dipole for various water depths d_1. Conductivity model of Fig. 1 with frequency $f = 0.5$ Hz.

The complete representation of the radial component E_r of a grounded horizontal electric dipole with TX at $\mathbf{r}_0$ and RX at $\mathbf{r}$ in cylindrical coordinates (r, φ, z) is

$$E_r(\mathbf{r}) = \int_0^\infty [\, Q_e(z|z_0,\kappa)\,(1/r) + Q_m(z|z_0,\kappa)\,\partial_r\,]J_1(\kappa r)\, d\kappa\, \cos\varphi, \tag{3}$$

where Q_e and Q_m describe, respectively, the contributions from TE- and the TM-mode. It is shown in Weidelt (2007)

- that due to the presence of the air-halfspace the TE-mode decays in powers of $1/r$ and
- that the TM-mode decays exponentially.

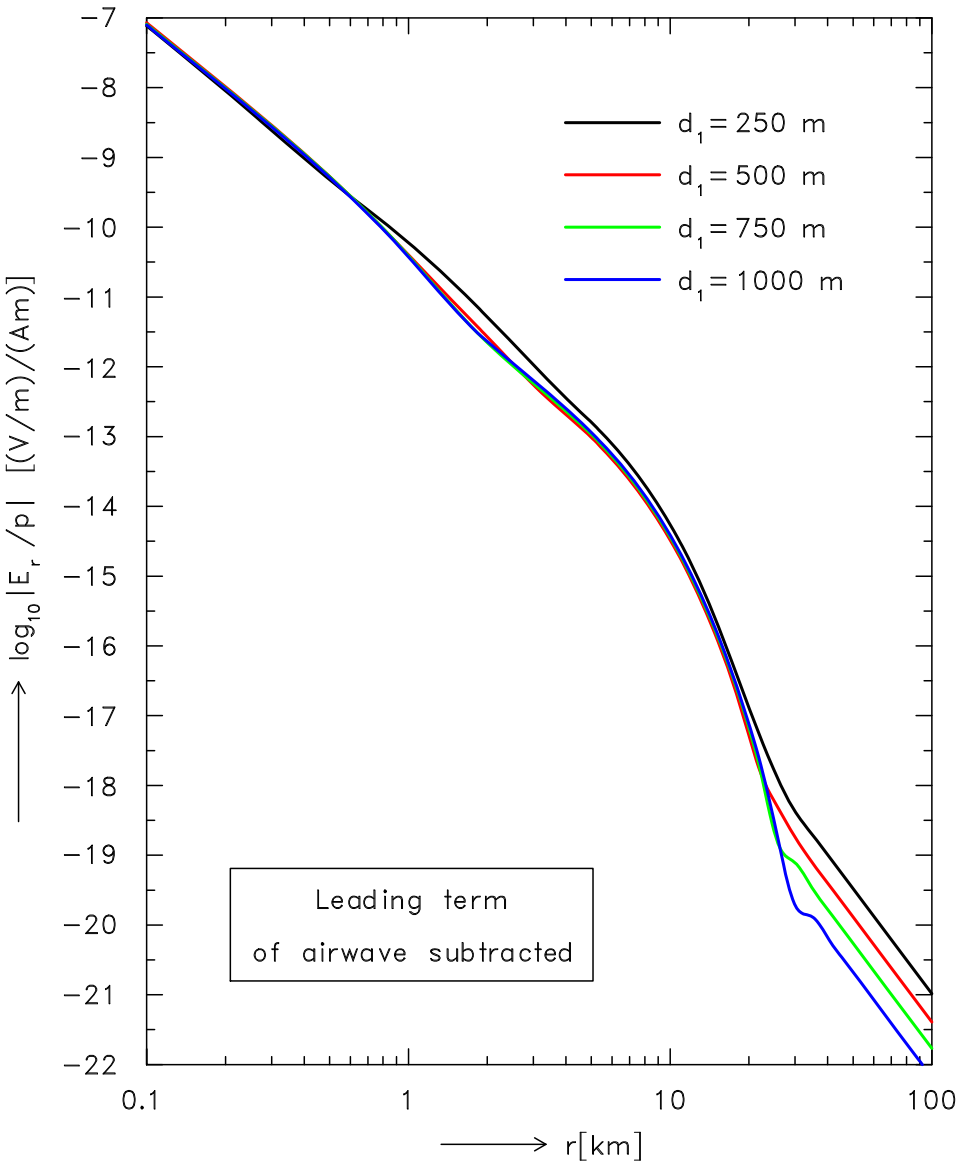

Figure 4: Subtraction of the leading airwave term from the data shown in Fig. 3. Now the resistive-layer mode becomes visible for all water depths d_1. The subtraction removes only the farfield with its $1/r^3$-decay, higher order terms $\sim 1/r^5$ evolve for $r > 20$ km. Air-ocean reflections with exponential decay, occurring at intermediate separations, are not eliminated.

The leading $1/r^3$ TE-mode term was given above. After the removal of the $1/r^3$ term, an asymptotic $1/r^5$-term appears, etc. The *complete airwave* removes all algebraic asymptotic terms $\sim 1/r^{2n+1}$ (see Fig. 5) and can be described in terms of the TE-mode: If the TE-mode part of E_r is given by

$$E_{er}(\mathbf{r}) = \int_0^\infty Q_e(z|z_0,\kappa) J_1(\kappa r)\, d\kappa,$$

then the complete airwave reads

$$E_r^{air}(\mathbf{r}) = \frac{1}{i\pi} \int_0^\infty [\, Q_e(z|z_0,+it) - Q_e(z|z_0,-it)\,] K_1(tr)\, dt, \tag{4}$$

with $J_1(\cdot)$ and $K_1(\cdot)$ as Bessel functions in conventional notation.

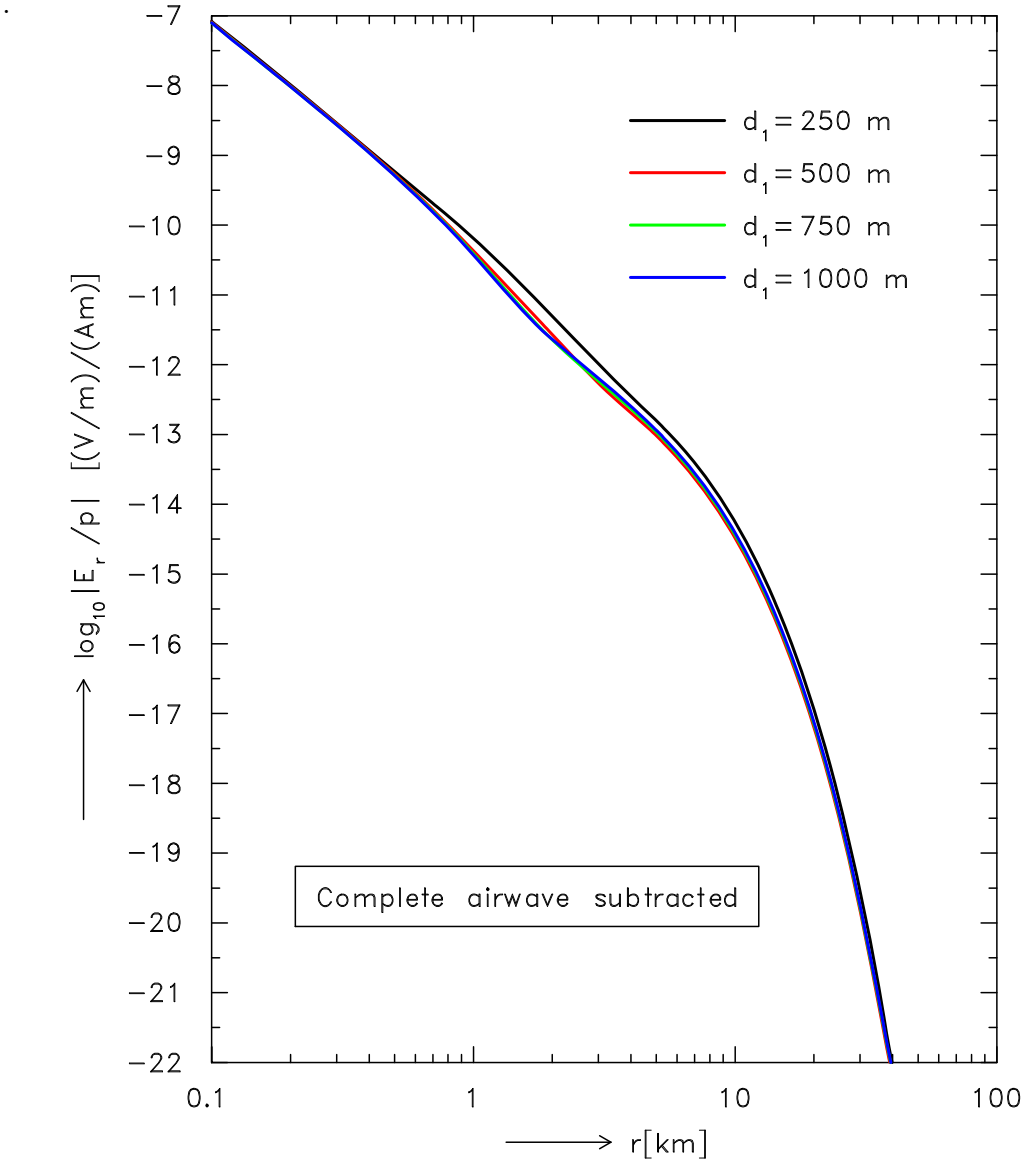

Figure 5: Subtraction of the complete airwave. The remainder approaches the exponentially decaying resistive-layer mode, see the blue lines in Figs. 6 and 12 (in the latter figure mostly coincident with the red line).

The successful removal of the airwave in Fig. 5 was possible only because we have assumed in Eqs. (1) and (4) a knowledge of the conductivity $\sigma(z)$. An approximate removal without recourse to $\sigma(z)$ is possible by observing in (1) that the leading term of the broadside configuration (E_φ at $\varphi = 90°$) is twice as large as that of the inline configuration (E_r at $\varphi = 0°$). Therefore, the quantity

$$E_r^{rem} := E_r(r, \varphi = 0°) - (1/2)E_\varphi(r, \varphi = 90°) \tag{5}$$

is free of the leading term of the airwave. Since the signal from the resistive layer is not present in the broadside component (see the bottom of Fig. 2), the difference field (5) is controlled in the farfield by the resistive layer mode and therefore presents a good approximation to the field obtained by removing the exact airwave (see Fig. 6).

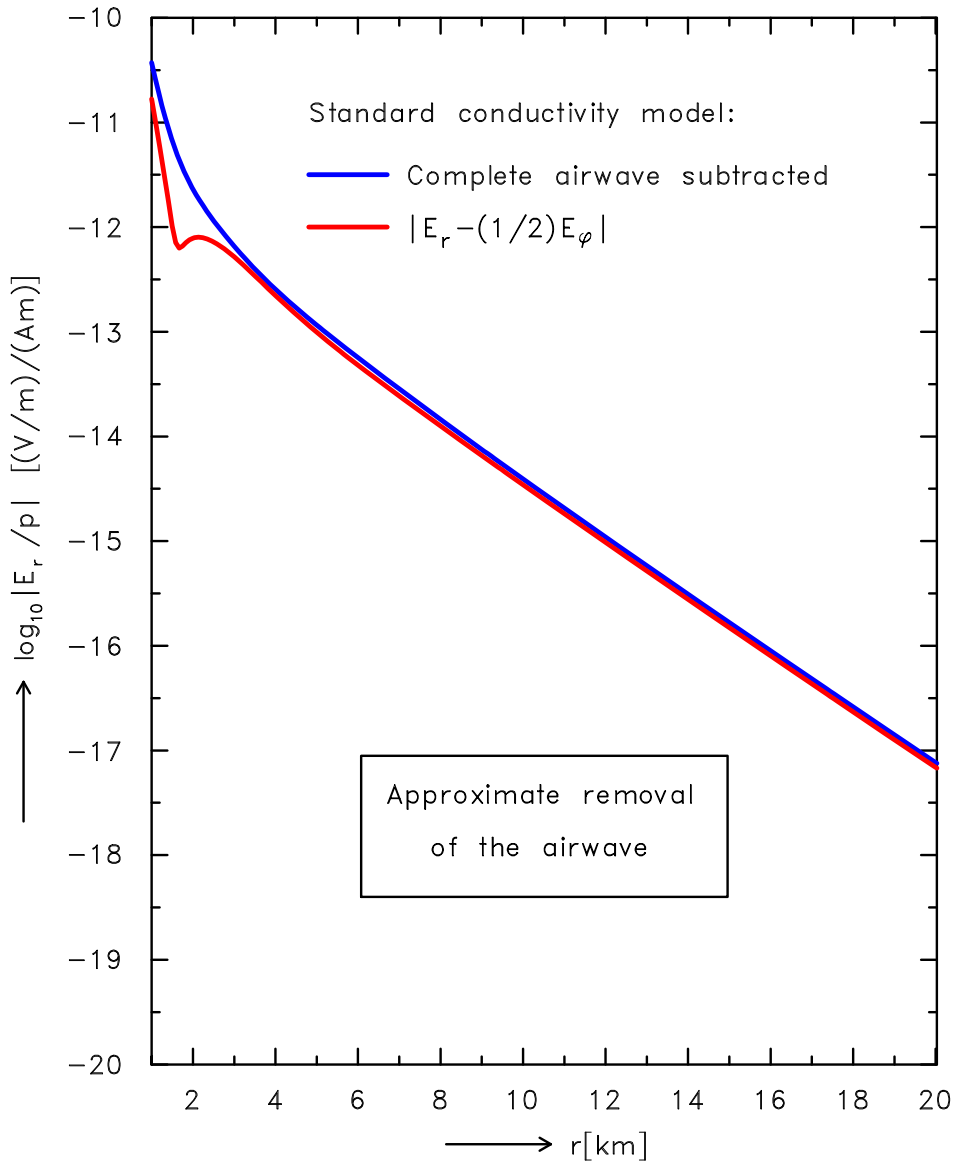

Figure 6: Approximate removal of the airwave according to Eq. (5). In the linear r-scale, the asymptotic exponential decay is evident in the blue line (corresponding to the blue line in Fig. 5).

3. The complex wavenumber plane

Usually, the field is obtained by superposing spectral terms with a real wavenumber κ in a Bessel function integral [as in (3)]. However, the extension of this superposition to complex wavenumbers clearly illuminates the nature of airwave and resistive-layer mode. If $f(\kappa)$ satisfies for real κ the symmetry $f(\kappa) = f(-\kappa)$, the extension from the positive κ-halfline to the complex upper κ-halfplane is performed via

$$\int_0^\infty f(\kappa) J_1(\kappa r)\, d\kappa = \frac{f(0)}{r} + \frac{1}{2} \int_{-\infty}^{+\infty} f(\kappa) H_1^{(1)}(\kappa r)\, d\kappa,$$

where $H_1^{(1)}(\cdot)$ is the Hankel function of first kind and first order. Above the indented real-line contour in Fig. 7 this function is analytic and decays exponentially.

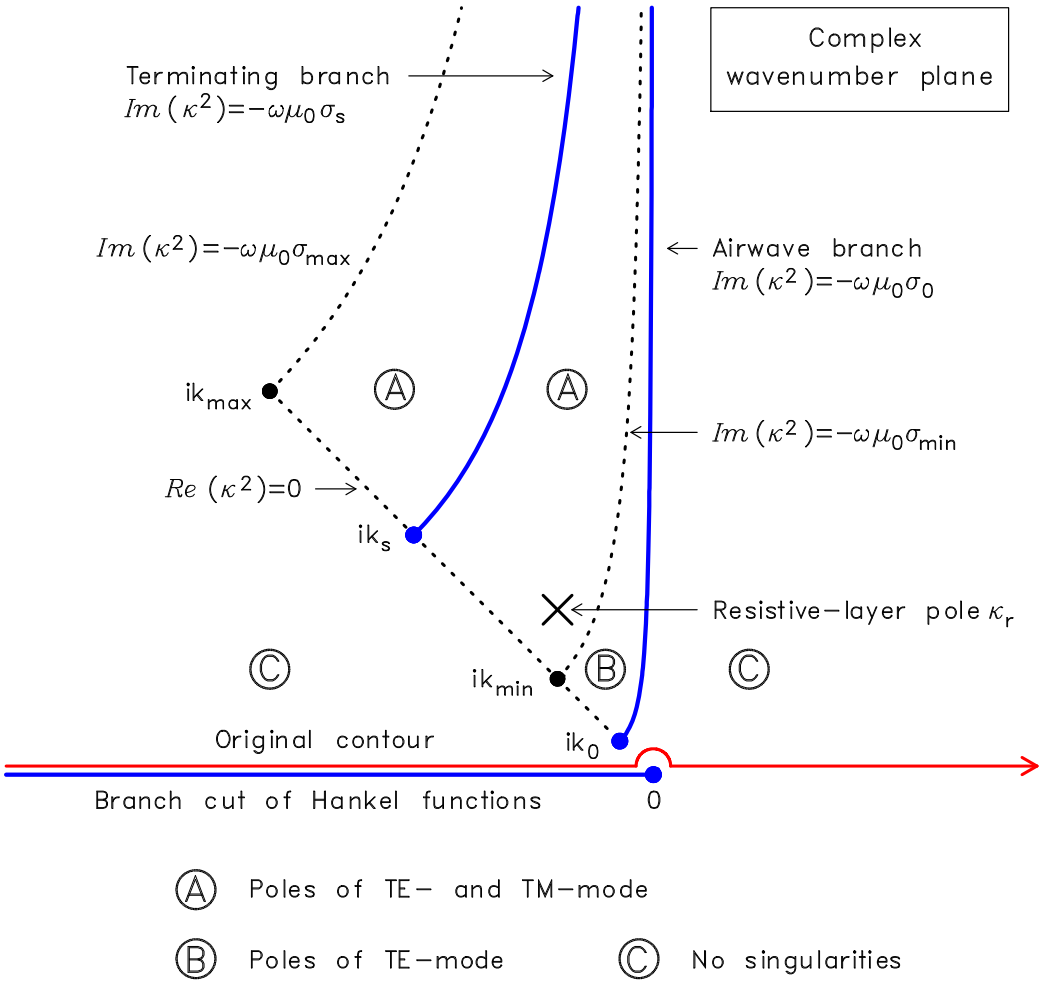

Figure 7: Analytical properties of the Bessel function integral kernel in the complex wavenumber plane. The full lines mark branch cuts. Inside the Earth the conductivity is assumed to vary in the limits $0 < \sigma_{min} \leq \sigma(z) \leq \sigma_{max} < \infty$. The branch points ik_0 and ik_s (referring to the limiting uniform halfspaces) and the endpoints ik_{min} and ik_{max} (referring to the limiting conductivities) are given by $\kappa = ik := (-1+i)\sqrt{\omega\mu_0\sigma/2})$. The situation near $\kappa = 0$ is disentangled by assigning to the air a small positive conductivity σ_0 and considering the limit $\sigma_0 \to 0^+$.

The analytical properties of the integration kernel allow to deform the original contour of Fig. 7 to the contour shown in Fig. 8. This contour is of advantage, if highly precise farfield data are required, since – apart from the airwave – only exponentially decaying terms are summed, whereas the contour along the real axis obtains the farfield by the unstable proces of destructive interference: For $r \to \infty$ each path element gives a contribution decaying exponentially $\sim \exp[-r\mathrm{Im}(\kappa)]$. The TM-mode contour can be closed already along the path $\mathrm{Im}(\kappa^2) = -\omega\mu_0\sigma_{min}$ (see Fig. 7) and therefore, the TM-mode is a superposition of contributions with a strict exponential decay. The critical point $\kappa = 0$ contributes only to the TE-mode, where the resulting decay in powers of $1/r$ forms the airwave.

First principles of the computation in the complex wavenumber domain for TE-mode sources are given by Kaufman & Keller (1983, p. 432-445) and Goldman (1990, Ch. 2).

The actual position of the poles in the complex κ-domain for the standard conductivity model of Fig. 1 is shown in Fig. 9 for $f = 0.5$ Hz. The *position* of the poles is an intrinsic feature of $\sigma(z)$ and f and is independent of the position of source and receiver. The *residual*, however, depends on the position.

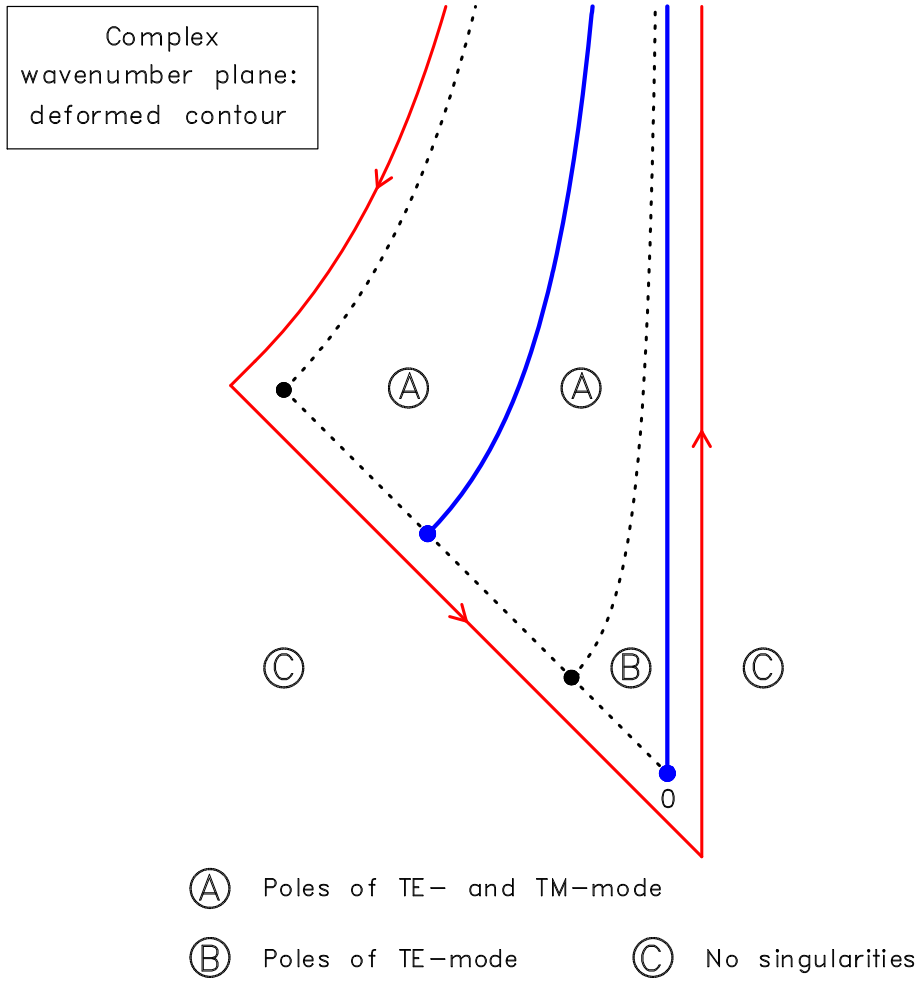

Figure 8: Deformation of the contour, originally confined to the real κ-axis (see Fig. 7), to a contour surrounding the region of singularities in the complex κ-plane. Contrary to Fig. 7, the air has again the conductivity $\sigma_0 = 0$. For $r \to \infty$ each path element gives a contribution decaying exponentially $\sim \exp[-r\mathrm{Im}(\kappa)]$. The TM-mode contour can be closed already along the path $\mathrm{Im}(\kappa^2) = -\omega\mu_0\sigma_{min}$ (see Fig. 7), and therefore the TM-mode is a superposition of contributions with a strict exponential decay. The critical point $\kappa = 0$ contributes only to the TE-mode, where the resulting algebraic decay in powers of $1/r$ forms the airwave.

Signatures of guided waves in the complex wavenumber plane are

- The 'airwave branch' (see Fig. 7) along the positive imaginary axis: The integral along both banks of the branch gives the complete pure airwave (4), considered as noise in marine CSEM.
- The resistive-layer pole κ_r: the residual at this point gives the resistive-layer mode, which is the signal of the target.

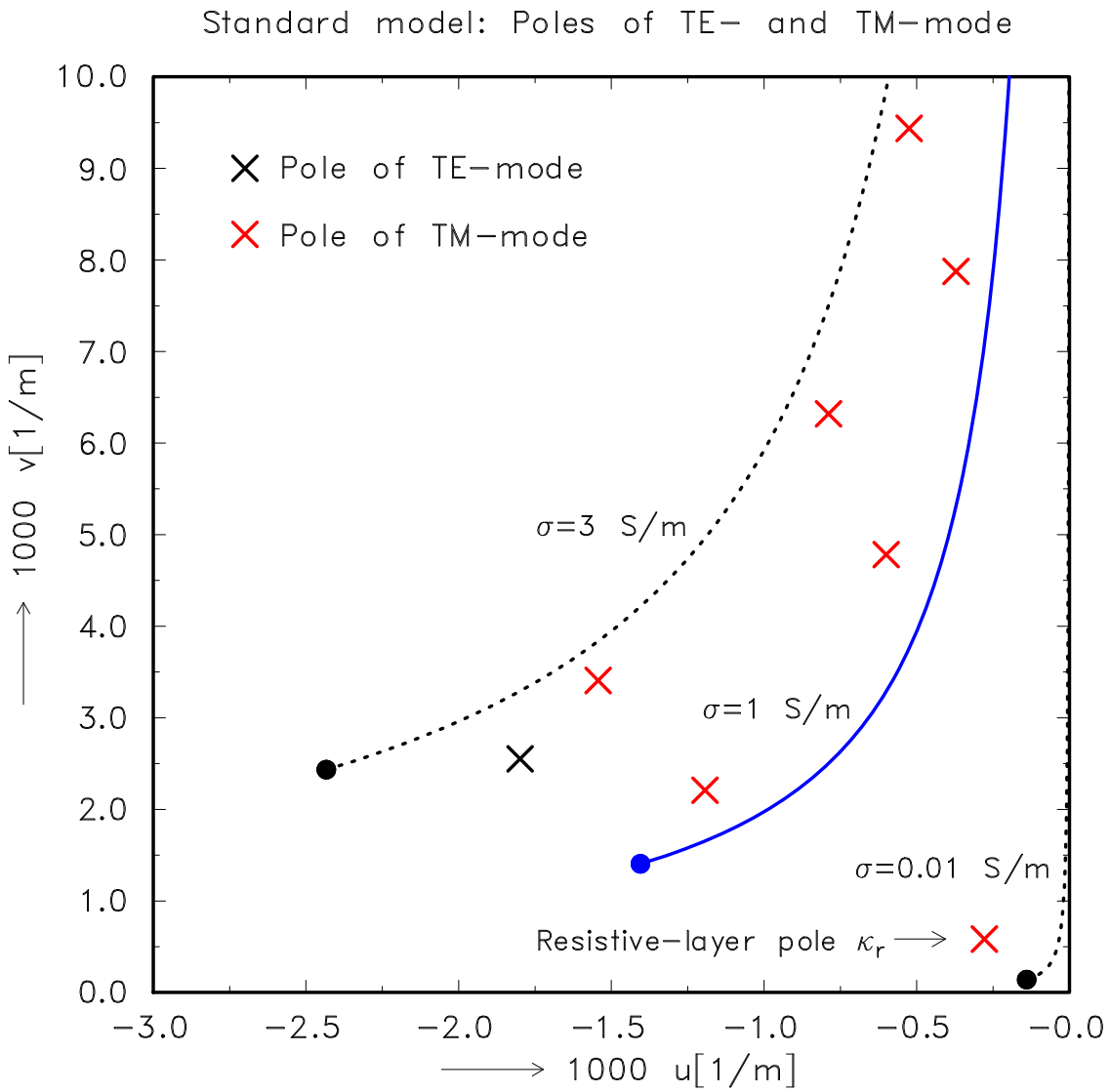

Figure 9: Actual position of the poles for the standard conductivity model of Fig. 1 in the complex plane $\kappa = u+iv$. The frequency is $f = 0.5$ Hz. Only the first six of an infinite number of TM-mode poles are shown. They describe highly damped reflections between air-ocean interface and the resistive layer. Also shown is the resistive-layer pole κ_r, an isolated TM-mode pole (close to the origin), which is responsible for the resistive-layer mode. – Note the different scales in u- and v-direction.

4. The resistive-layer mode

For general κ, the differential equation for the spectral TM-mode potential $f_m(z,\kappa)$,

$$\sigma(z)[\, f_m'(z)/\sigma(z)\,]' = [\kappa^2 + i\omega\mu_0\sigma(z)\,]f_m(z)$$

has as two *linearly independent* solutions an upward propagating solution $f_m(z) =: f_{ma}(z)$ vanishing for $z \to 0$ and a downward propagating solution $f_m(z) =: f_{mb}(z)$ vanishing for $z \to \infty$. At the poles of the TM-mode integral kernels, e.g. at $\kappa = \kappa_r$, the solutions become *linearly dependent*, such that

$$f_{ma}(z,\kappa_r) = f_{mb}(z,\kappa_r) =: f_{mr}(z)$$

is an eigensolution, which decays for $z \to 0$ and for $z \to \infty$. This particular eigensolution, with its peak amplitude in the resistive layer, is the *resistive-layer mode*. It is displayed in Fig. 10. Physically, $f_m(z,k)$ is proportional to the spectral vertical current density $J_z(z,\kappa)$ [therefore $f_{ma}(0,\kappa) = 0$].

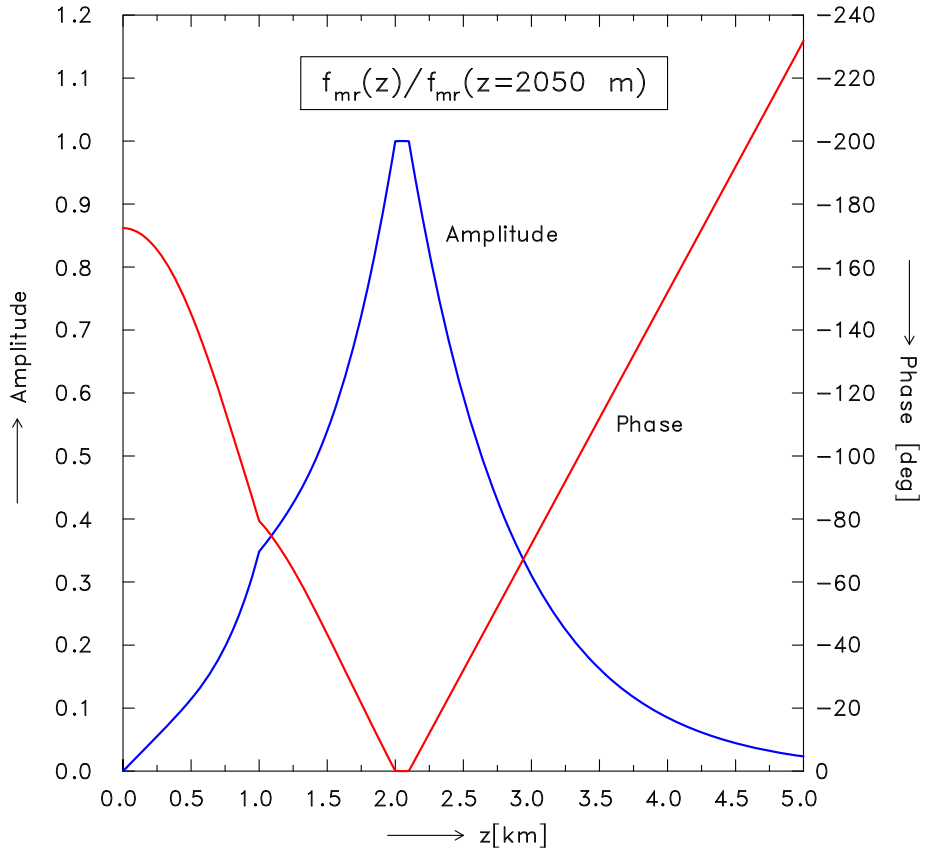

Figure 10: The eigensolution $f_{mr}(z)$ of the resistive-layer mode for the standard conductivity model of Fig. 1. The slope discontinuities at $z = 1$ km mark the seafloor.

.

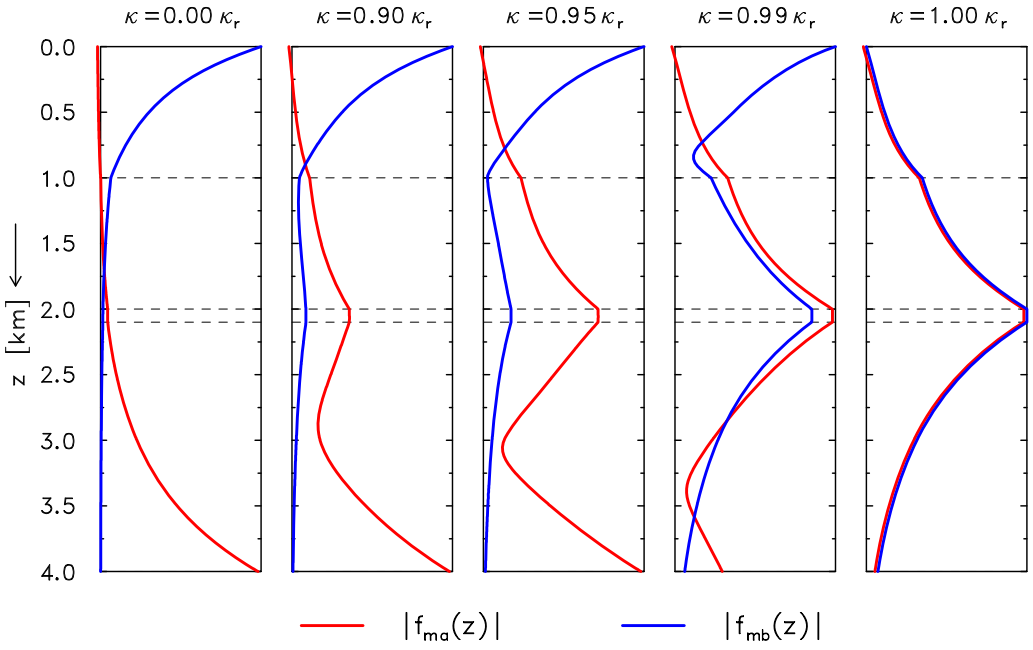

Figure 11: The transition from linear independence to linear dependence when approaching $\kappa = \kappa_r$ along a straight line from the origin $\kappa = 0$. The dotted lines mark the layer boundaries.

The resistive-layer pole lies at

$$\kappa_r = (-2.788726 + i\,5.831761) \cdot 10^{-4}\mathrm{m}^{-1},$$

corresponding to a scale length of

$$L_r = 1/\mathrm{Im}(\kappa_r) = 1714.75 \text{ m}.$$

The resistive-layer mode $E_r^{rlm}(\mathbf{r})$, which is the residual at κ_r, is shown in Fig. 12 as the red line. Apart from a factor, independent of the position of TX and RX, it is given by

$$E_r^{rlm}(\mathbf{r}) \sim \frac{f'_{mr}(z) f'_{mr}(z_0)}{\sigma(z)\sigma(z_0)} \cdot \partial_r H_1^{(1)}(\kappa_r\, r) \cos\varphi.$$

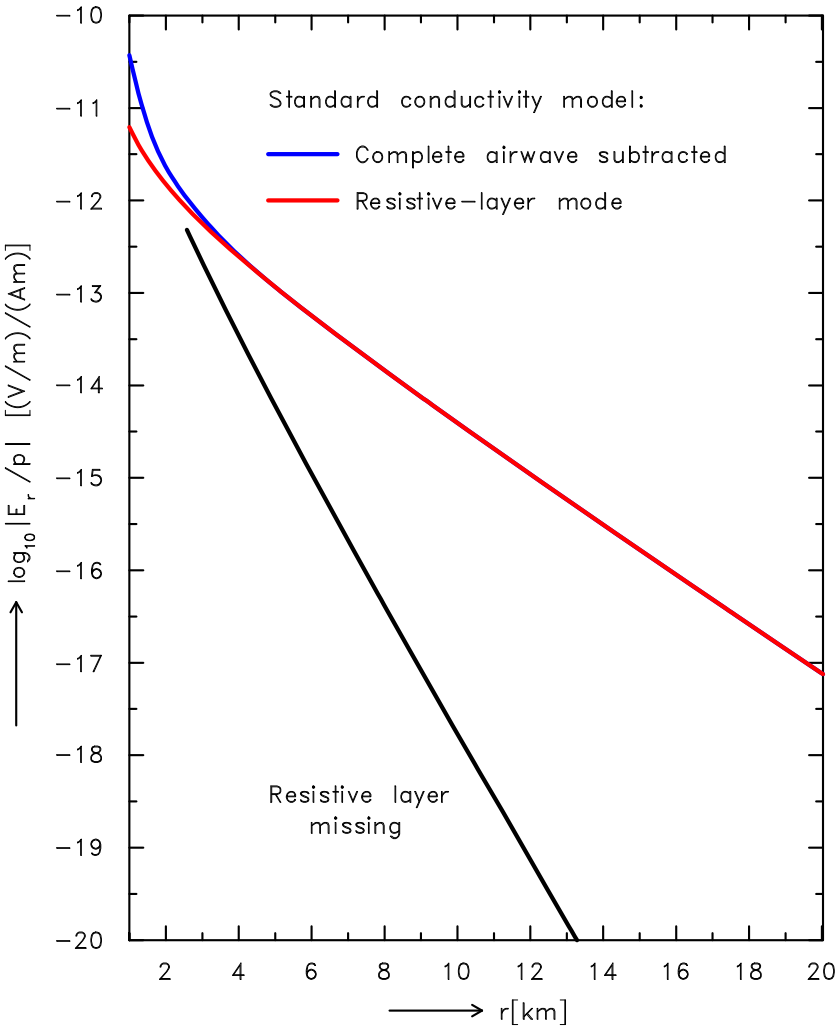

Figure 12: The blue line (coinciding in the farfield with the red line) represents the same information as the blue lines in Figs. 5 and 6. In the linear r-scale the asymptotic exponential character becomes obvious. The farfield agreement with the resistive-layer mode (red line) shows that the latter provides an excellent farfield approximation of E_r freed from the airwave. After the removal of the airwave, the distinction from a model without the resistive layer becomes easily possible.

5. The adjustment distance in MT

If $\sigma(z) > 0$ in $z > 0$, all horizontal components of the electric and magnetic field decay at great separations r between TX and RX for magnetic dipoles (HMD and VMD) and for horizontal electric dipoles $\sim 1/r^3$. Therefore the surface impedance as ratio beqween orhogonal components of **E** and **H** tends at great separations to the plane-wave limit. The scale length lor reaching this limit is the adjustment distance L_a. In general, L_a is in the order of the modulus Scmucker's complex inductive scale length $c(\omega)$, defined for a layered earth as

$$c(\omega) := c(0,\omega) \quad \text{and} \quad c(z,\omega) := -E_h(z,\omega)/E_h'(z,\omega).$$

Here E_h is a horizontal electric field component. There is a notable exception, however, where the farfield will start at considerably greater separations. This is – in the simplest case – a three-layered earth with a (thick) resistive layer sandwiched between a (thin) conductive overburden and a conductive substratum. The corresponding conductivity model is shown in Fig. 13.

Adjustment distance: Typical conductivity model

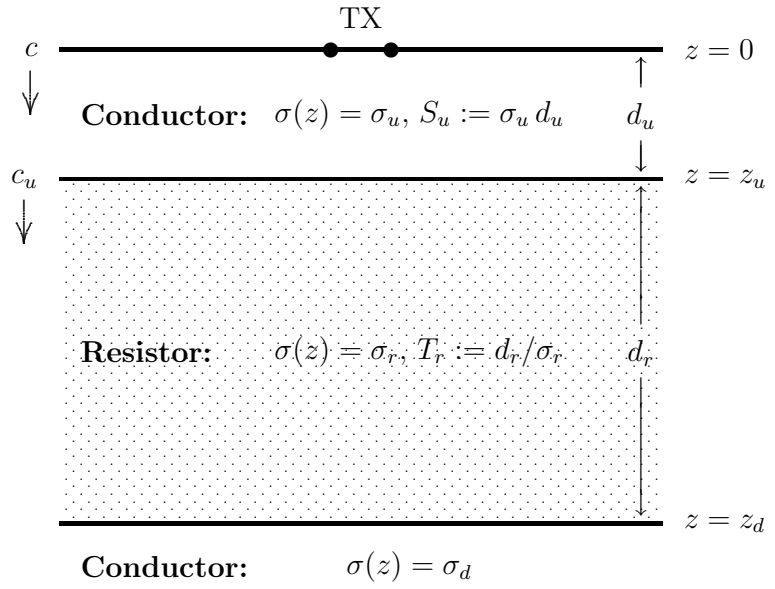

DC-estimate of adjustment distance (Ranganayaki & Madden 1980):

$$L_a \approx \sqrt{S_u\, T_r}$$

Inductive estimate of adjustment distance (Fainberg & Singer 1987):

$$L_a = \frac{1}{\mathrm{Im}(\kappa_a)} \approx \frac{\sqrt{S_u\, T_r}}{\mathrm{Re}\sqrt{c_u/c}} \leq \sqrt{S_u\, T_r}$$

$$\kappa_a^2 \approx -\frac{c_u/c}{S_u\, T_r}$$

Figure 13: Conductivity model and experimental setup, in which the plane-wave impedance is reached only at great separations, essentially due to 2D propagation at small and moderate separations.

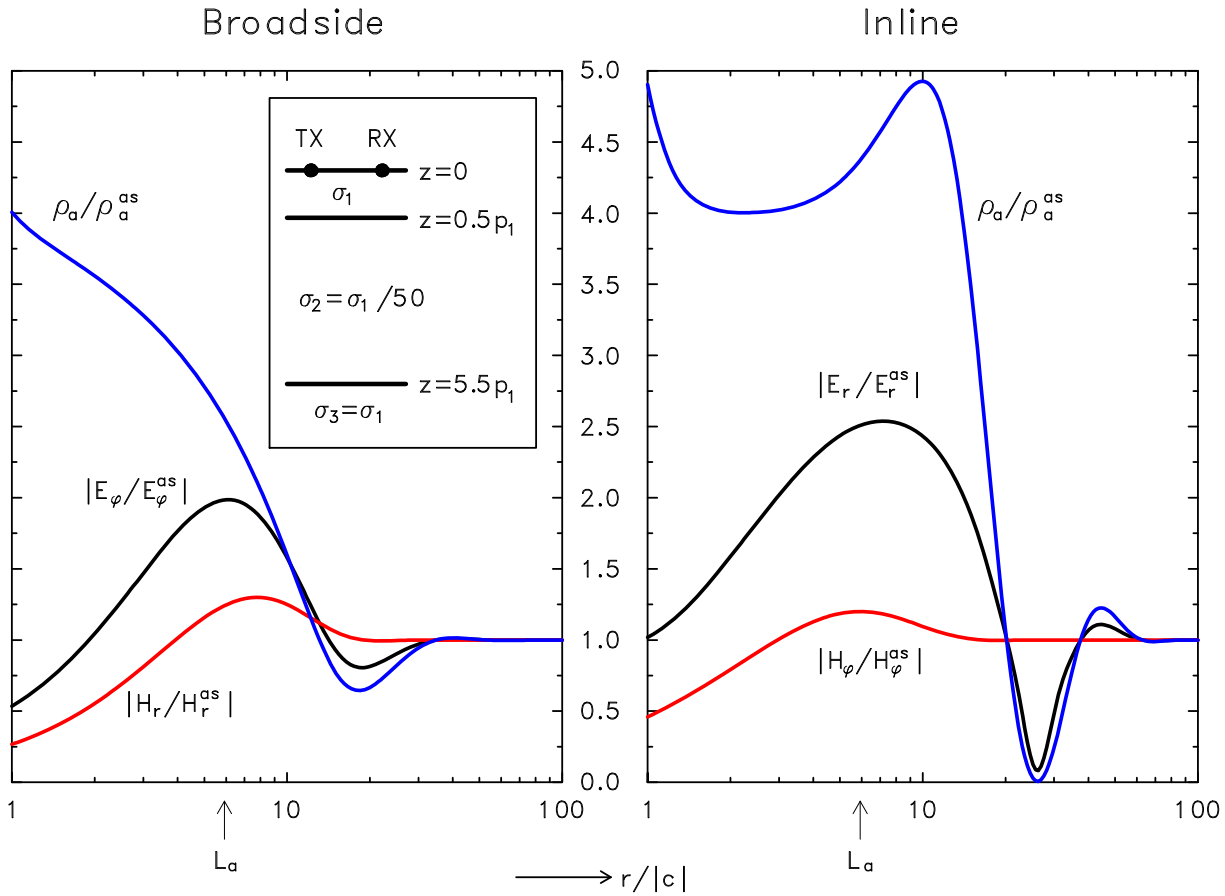

Figure 14: Horizontal electric and magnetic field components of a HED, normalised with their asymptotic values (superscript *as*) decaying $\sim 1/r^3$ (= airwave). Because of the $1/r^2$-decay of E_ϕ and E_r at small and intermediate separations, the *normalized* values of the electric field components increase with r up to $r \approx L_a$ and then sharply decrease because of the exponential decay of the TM-mode part.

The source is a HED in or on the conductive overburden. Due to the galvanic contact, the currents are at small and moderate distances confined to the conductive overburden. The reduced dimensionality leads to TM-mode electric dipole fields decaying first only $\sim 1/r^2$. At greater separations the vertical electric currents of the source dipole will penetrate the resistive central layer. When sensing the conductive substratum, the TM-mode currents decay exponentially rather than $\sim 1/r^2$. This exponential TM-mode decay is valid under the assumption that $\sigma(z) > 0$ in $z > 0$. If this condition is violated by a perfectly *insulating* intermediate layer, the $1/r^2$-decay of the TM-mode field would perpetuate for all separations. If this condition is satisfied only marginally by a (highly) resistive intermediate layer, the exponential decay would be present, but would start at great separation, which is quantified by the *adjustment distance* L_a. The galvanic currents will stay the longer in the conductive overburden the better the overburden conductivity σ_u and the smaller the resistive-layer conductivity σ_r. At separations $r \gg L_a$, the TM-mode electric field has diappeared and TE-mode part, decaying always $\sim 1/r^3$, will prevail.

The consideration of the adjustment distance will certainly be relevant for Controlled Source Audio Magnetotellurics (CSAMT) over a conductivity structure of the type sketched in Fig. 13. Moreover, the adjustment distance plays also a role in ordinary MT, since the anomalous electric fields caused by lateral conductivity heterogeneities can be represented as a superposition of HED fields with sources in the anomalous domain and with amplitudes controlled by the conductivity contrast.

For MT the first estimate of L_a was given by Ranganayaki & Madden (1980), who showed that

$$L_a \approx \sqrt{S_u\, T_r}, \tag{6}$$

where $S_u := \sigma_u\, z_u$ is the conductance of the overburden and $T_r := d_r/\sigma_r$ is the integrated resistivity of the intermediate layer (see Fig. 13). The simple and useful estimate (6) reflects already correctly the dependence on σ_u and σ_r as anticipated above. It is a direct current approximation, which does not yet take induction into account. This was first achieved in the approximation of Fainberg & Singer (1987), who relate L_a to the TM-mode pole κ_a with the smallest imaginary part. This pole is approximately positioned at

$$\kappa_a^2 \approx -\frac{c_u/c}{S_u\, T_r}, \tag{7}$$

such the exponential radial decay $\sim \exp[\,-r\mathrm{Im}(\kappa_a)\,]$ yields

$$L_a = \frac{1}{\mathrm{Im}(\kappa_a)} \approx \frac{\sqrt{S_u\, T_r}}{\mathrm{Re}\sqrt{c_u/c}}. \tag{8}$$

Here c and c_u are the inductive scale lengths at $z = 0$ and $z = z_u$, respectively. Approximately we have

$$c_u/c \approx 1 + i\omega\mu_0\, S_u\, c_u. \tag{9}$$

Since $\mathrm{Im}(c_u) < 0$, Eq. (9) implies $\mathrm{Re}\sqrt{c_u/c} \geq 1$. Therefore the consideration of induction according to (8) and (9) leads to a reduction of the DC estimate (6). A numerical example will be given below.

The adjustment distance is illustrated in the simple example of Fig. 14. The source is a HED at $z = 0$. The left panel shows the *broadside* configuration (with bipoles of TX and RX pointing into the figure) and the right panel shows the *inline* configuration (with TX and RX bipoles in the plane of the figure). The field components are normalized by their asymptotic farfield values, denoted by the superscript as. Up to separations $r \approx L_a$, the normalized electric field increases with r because E is dominated by the TM-mode part decreasing $\sim 1/r^2$, whereas $E^{as} \sim 1/r^3$. For $r > L_a$, the exponential decrease of the TM-mode leads to a sharp decrease of E, which passes through a pronounced minimum before it is well presented by its asymptotic values. In the present model, E_ϕ and E_r reach the asymptotic regime only for $r \approx 40|c|$ and $r \approx 50|c|$, respectively. Shown are also the corresponding normalized apparent resistivities ϱ_a/ϱ_a^{as}. The reason for the pronounced minimum will be discussed below.

In the present example, the DC estimate (6) yields $L_a/|c| = 11.31$. The reduction of this estimate due to induction is remarkable: The Fainberg-Singer estimate gives $L_a/|c| = 5.61$, which is not too different from the true value $L_a/|c| = 5.92$, obtained by exactly determining the κ_a as the pole with the smalles imaginay part (see Fig. 15).

Taking again the model of Fig. 14 as an example, Fig. 15 shows both the exact locations of the first six TM-mode poles and the line $\mathrm{Im}(\kappa^2) = -\omega\mu_0\sigma_r = -\omega\mu_0\sigma_2$, on which the poles are located for the case that the resistive layer is sandwiched between two *perfect* conductors. The separation of poles decreases for increasing thickness d_r of the resistive layer and increases for decreasing thickness. Therefore, only the single pole κ_r is present in the marine CSEM model with a *thin* resistive layer (see Fig. 9). Fig. 15 shows also the first six poles of an infinite sequence of TE-mode poles. In particular the TE-mode pole with the smallest imaginary part plays a role for the decay of the E-field at intermediate distances, but finally the leading TE-mode term from the airwave branch will dominate the pole contributions.

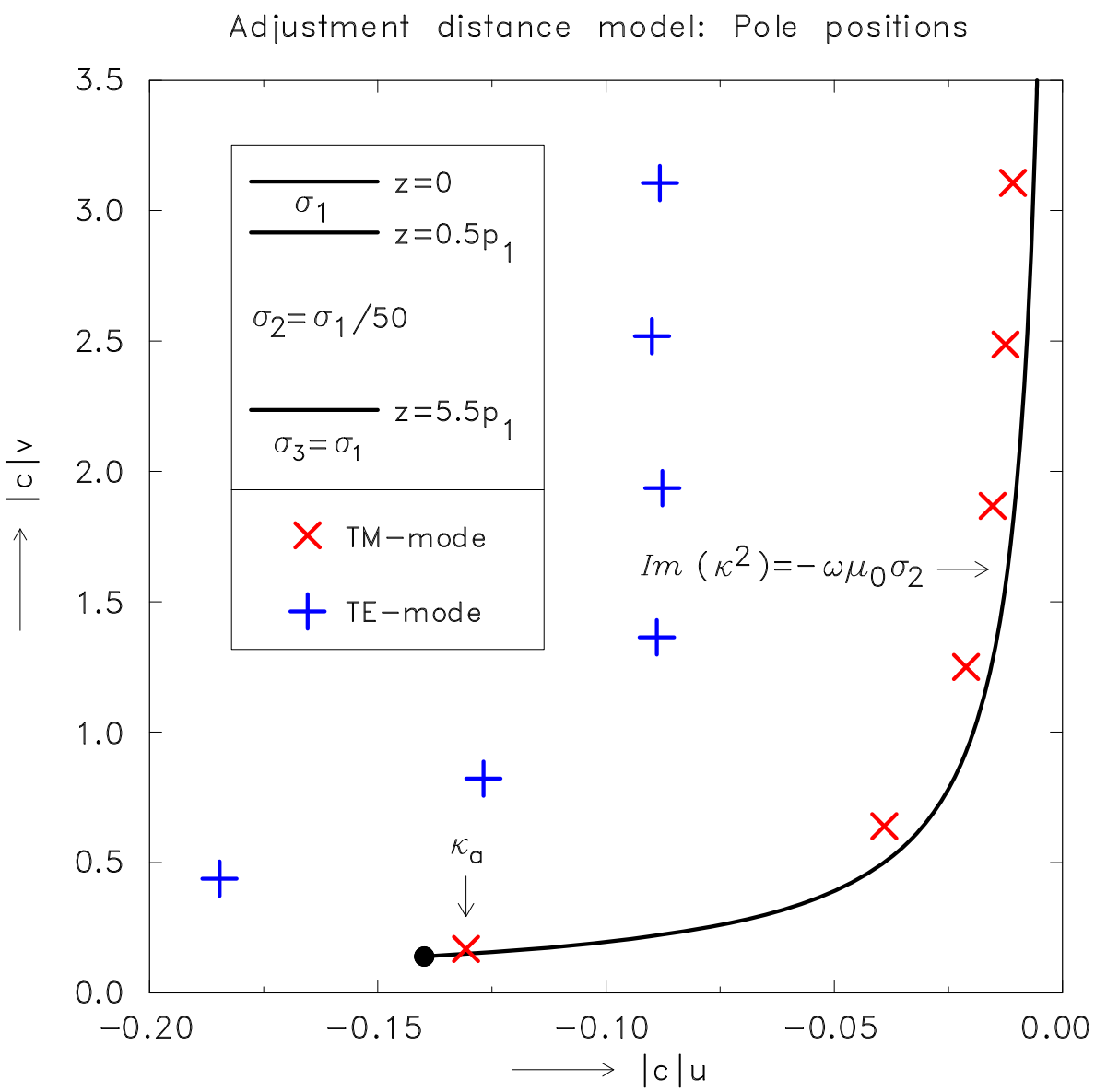

Figure 15: TM- and TE-mode poles for the conductivity model assumed in Fig. 14 and repeated here for convenience. The TM-mode pole κ_a gives rise to the adjustment distance $L_a = 1/\mathrm{Im}\kappa_a$. The line $\mathrm{Im}(\kappa^2) = -\omega\mu_0\sigma_2$ corresponds to the line $\mathrm{Im}(\kappa^2) = -\omega\mu_0\sigma_{min}$ in Fig. 7. Note the different scales in u- and v-direction.

At the pronounced $|E_r|$-minimum at $r/|c| \approx 26$, the contributions from TE- and TM-mode are approximately of the same size, but of different sign, $E_r^{(e)}/E_r^{(m)} = -1.053 + i\,0.068$, such that the contributions almost annihilate.

The *tertium comparationis* between the resistive-layer mode in CSEM and the adjustment distance in MT is a resistive layer sandwiched beween two conductive layers, which in both cases gives rise to pronounced energy propagation in the resistor with well-defined long decay length L_r and L_a. Both scale lengths are associated with a TM-mode pole close to the origin $\kappa = 0$. The airwave in CSEM corresponds to the asymptotic behaviour of the MT fields. Whereas unwanted noise CSEM, the asymptotic field provides a safe reference in MT.

Facit

- The contribution discusses the relevant guided waves in marine CSEM with restriction to frequency sources and electric fields for 1D conductivity models. The emphasis lies on fundamental principles rather than on practice orientation. The results are given without an attempt of an explicit derivation.
- A simple general expression is given for the leading term of the airwave for an arbitrary 1D conductivity distribution.
- Working in the complex wavenumber domain and locating poles and branch points allows
  - to isolate the complete airwave and the resistive-layer mode;
  - to compute highly precise farfield data;
  - to infer immediately that TM-mode contributions will decay exponentially, wheras TE-mode contributions may show a decay in powers of $1/r$;
  - to quantify decay lengths of individual field components.
- Fig. 12 shows that – for a representative model – the superposition of airwave and resistive-layer mode provides an excellent description of the electric field over a wide range of separations.
- For the model with a sandwiched resistor between conductors, an intimate connection is established between between CSEM and MT, where the TM-mode pole with the smallest imaginary part defines the appropriate scale length of radial decay. This is strictly valid only for CSAMT, but is of relevance also for the *anomalous* fields of lateral conductivity anomalies generated by plane-wave sources (as assumed in MT).

References

Fainberg, E.B. & Singer, B.Sh., 1987. The influence of surface inhomogeneities on deep electromagnetic soundings of the Earth, *Geophys. J. R. astr. Soc.*, **90**, 61-73.

Goldman, M.M., 1990. Non-conventional methods in geoelectrical prospecting, Ellis Horwood Series in Applied Geology, Ellis Horwood Ltd., New York, Ch. 2.

Kaufman, A.A. & Keller, G.V., 1983. Frequency and transient sounding, Methods in Geochemistry and Geophysics, vol. 16, Elsevier, Amsterdam, p. 432-445. Ltd., New York, Ch. 2.

Ranganayaki, R.P. & Madden, T.R., 1980. Generalized thin sheet analysis in magnetotellurics: an extension of Price's analysis, *Geophys. J. R. astr. Soc*, **60**, 445-457.

Weidelt, P., 2007. Guided waves in marine CSEM, *Geophysical J. Int.*, **171**, 153-176.